processes

MDPI

Article

New Method for Calculating Rock Compressibility, Dynamic Reserves, and Aquifer Size for Fractured–Vuggy Reservoirs with Bottom Aquifer

Bo Fang [1,*], Yuwei Jiao [1], Qi Zhang [1], Yajie Tian [1], Baozhu Li [1] and Wei Yu [2]

[1] Research Institute of Petroleum Exploration & Development, Beijing 100083, China; jiaoyuwei@petrochina.com.cn (Y.J.); zhangqiq@petrochina.com.cn (Q.Z.); tianyajie0508@petrochina.com.cn (Y.T.); lbz@petrochina.com.cn (B.L.)
[2] SimTech LLC, Houston, TX 77084, USA; yuwei127@gmail.com
* Correspondence: fb_work@petrochina.com.cn or fb_work@sina.com

Abstract: Due to the complex reservoir types and strong heterogeneity of fractured–vuggy reservoirs with aquifers, evaluating such reservoirs' dynamic reserves and aquifer size is challenging. This paper established a segmented elastic-drive material balance equation based on the material balance principle by combining the functional relationships among the crude oil volume factor, crude oil compressibility, and formation pressure. The PELT algorithm was used to segment the water invasion stages, and nonlinear least squares fitting was employed to determine the rock compressibility, dynamic reserves, and aquifer size of fractured–vuggy reservoirs. This study shows that production in fractured–vuggy reservoirs with aquifers can be divided into three stages: no water invasion, initial water invasion, and full water invasion. Rock compressibility and dynamic reserves can be calculated using production data from the no water invasion stage, while the aquifer size can be determined from data in the water invasion stage. Influenced by connectivity and production regulations, aquifers may not be fully affected by pressure waves, causing the aquifer size to increase gradually until stabilization. Compared with numerical simulation data, the method presented in this paper achieves errors of 0.34%, 0.67%, and 1.19% for rock compressibility, dynamic reserves, and aquifer size, respectively.

Keywords: fractured–vuggy carbonate reservoir; rock compressibility; dynamic reserves; aquifer size; improved material balance method

check for updates

Academic Editor: Michael C. Georgiadis

Received: 5 February 2025
Accepted: 24 February 2025
Published: 27 February 2025

Citation: Fang, B.; Jiao, Y.; Zhang, Q.; Tian, Y.; Li, B.; Yu, W. New Method for Calculating Rock Compressibility, Dynamic Reserves, and Aquifer Size for Fractured–Vuggy Reservoirs with Bottom Aquifer. *Processes* **2025**, *13*, 684. https://doi.org/10.3390/pr13030684

Copyright: © 2025 by the authors. Licensee MDPI, Basel, Switzerland. This article is an open access article distributed under the terms and conditions of the Creative Commons Attribution (CC BY) license (https://creativecommons.org/licenses/by/4.0/).

1. Introduction

The reservoir spaces of fractured–vuggy carbonate reservoirs are highly diverse, including fractures, caves, and combinations thereof. These reservoirs exhibit uneven spatial distribution, significant randomness, and complex connectivity, making it challenging to obtain reservoir parameters and evaluate dynamic reserves [1–4]. To address the complex fluid flow behavior in fractured–vuggy reservoirs, researchers have proposed well test and numerical simulation methods based on seepage and fluid mechanics to estimate reserves [5–11]. However, current simplified physical models for well tests cannot accurately describe actual reservoir characteristics, while coupled free-flow and seepage numerical simulation models are computationally intensive and unsuitable for field applications. Water invasion models commonly used in unsteady- or pseudo-steady-state water invasion models require numerous known parameters, limiting their application in fractured–vuggy

reservoirs. Material balance methods based on macroscopic principles overcome the challenges of describing complex microscopic flow behaviors and have significant advantages in evaluating key parameters of fractured–vuggy reservoirs [12–16].

Istayeva and King [17] proposed a modified dynamic material balance method to calculate the dynamic reserves of ultra-large carbonate reservoirs. This method can estimate geological reserves without the static pressure obtained from the shut-in test but cannot calculate the size of water bodies. Han et al. [18] established a novel flow material balance method for determining dynamic reserves; however, the governing equation derived from traditional linear seepage mechanics theory proved inadequate in accurately describing the production characteristics of oil wells in fractured–vuggy reservoirs. Yao et al. [19] integrated linear and logarithmic water invasion models with mass balance equations to iteratively resolve and calculate dynamic reserves and the size of the water body. It is important to note that the water invasion characteristics of fractured–vuggy reservoirs are influenced by geological parameters, suggesting that various water invasion models may exist.

Another effective methodology for calculating dynamic reserves involves constructing a material balance model utilizing water injection data [20,21]. Yue et al. [22] proposed a new water injection indicator curve model that uses a multi-round water injection curve to ascertain the volumes of crude oil and water. Wang et al. [23] introduced an enhanced water injection indicator curve that incorporates the original oil–water ratio to calculate dynamic reserves, considering the different fracture–vug assemblages within the fractured–vuggy carbonate reservoirs of the Tahe oilfield. Zhang et al. [24] combined the degree of reservoir pressure recovery, the water cut, and various boundary conditions to formulate a mathematical model for evaluating dynamic reserves, taking into consideration the oil–water volume ratio. Nonetheless, a major limitation of this approach is the absence of water injection data for fractured–vuggy reservoirs during early depletion processes.

Rock compressibility is also a critical parameter in the material balance equation. Yildiz [25] introduced a graphical method for predicting rock compressibility utilizing production data. This method entails converting the material balance equation into various line formats and employing the intercept and slope of the resulting lines to ascertain rock compressibility. However, this method is exclusively applicable to reservoirs with aquifers. Based on seepage mechanics, Kegang et al. [26] proposed a technique for calculating rock compressibility using experimental permeability data. The accuracy of this model, however, is significantly contingent upon the precision of other parameters. Zhu et al. [27] presented a theoretical method to calculate rock compressibility by using the rock's Poisson ratio, elastic modulus, and porosity. Nonetheless, this model does not apply to reservoirs with considerable heterogeneity.

In conclusion, there remains a deficiency in comprehensive methodologies for determining key parameters of unsaturated fractured–vuggy reservoirs with aquifers where rock compressibility is unknown. This paper introduces a modified elastic-drive material balance equation with piecewise fitting. First, a segmented material balance equation is established, accounting for elastic energy contributions from oil, rock, and water during distinct production stages. Next, the PELT algorithm is applied to divide water invasion into stages, followed by nonlinear least squares optimization to calculate key parameters. Finally, the method is validated via data fitting with a numerical simulation model. A field case illustrates the method's practicality, revealing a gradual increase in aquifer size due to delayed pressure propagation. This approach provides a computationally efficient, high-precision tool for evaluating complex fractured–vuggy reservoirs, bridging the gap between theoretical models and field operations.

2. The Establishment of the Material Balance Equation

Due to the complex connected system in fractured–vuggy reservoirs, water invasion may not occur immediately during reservoir development. Therefore, when formulating the material balance equation, it is imperative to account for both the no water invasion stage and the water invasion stage. Furthermore, in contrast to traditional material balance methods, this paper proposes an improved method that considers the effects of changes in oil properties resulting from significant pressure drops.

2.1. No Water Invasion Stage

At the no water invasion stage, oil and water production is derived from the elastic energy of the crude oil, pores, and water in the oil region. Therefore, according to material balance theory, the following equation can be obtained:

$$N_p B_o + W_p B_w = N B_{oi}(p_i - p)\left(C_{o,avg} + \frac{C_f + C_w S_{wi}}{1 - S_{wi}}\right) \tag{1}$$

where N_p is the cumulative oil production, m^3; B_o is the oil volume factor; W_p is the cumulative water production, m^3; B_w is the water volume factor; N is the original oil in place, m^3; B_{oi} is the oil volume factor in the initial state; p_i is the initial formation pressure, MPa; p is the average formation pressure, MPa; $C_{o,avg}$ is the average oil compressibility, MPa^{-1}; C_f is the rock compressibility, MPa^{-1}; C_w is the water compressibility, MPa^{-1}; and S_{wi} is the water situation at the initial stage.

According to the experimental data fitting study by Vazques and Beggs [28], the calculation formula for the crude oil compressibility coefficient is as follows:

$$C_o = \frac{a_1 + a_2 R_s + a_3\left(5.625 \times 10^{-2} T + 1\right) + a_4 \gamma_{gs} + a_5\left(\frac{1.076}{\gamma_o} - 1\right)}{a_6 p} \tag{2}$$

where a_i is the calculation parameter; R_s is the dissolved gas–oil ratio; T is the temperature, K; γ_{gs} is the relative density of separated gas in the separator; and γ_o is the relative density of the surface degassing crude oil.

When the formation pressure is higher than the bubble point pressure, the dissolved gas–oil ratio of the unsaturated reservoir is unchanged, and T, γ_{gs}, and γ_o are also constant. Therefore, the parameters independent of pressure (p) can be consolidated into a constant term (b), allowing Equation (2) to be simplified as

$$C_o = \frac{b}{p} \tag{3}$$

The known relationship between the oil volume factor and oil compressibility as follows:

$$C_o = -\frac{1}{B_o}\frac{dB_o}{dp} \tag{4}$$

By combining Equation (3) and Equation (4), the following equation is obtained:

$$\int \frac{b}{p} dp = \int \frac{1}{B_o} dB_o \tag{5}$$

and we can derive the following result by taking the logarithm of both sides:

$$B_o = e^{b \ln p + Con} = e^{Con} \cdot p^b = a \cdot p^b \tag{6}$$

Therefore, the oil volume factor can be regarded as a power function of pressure. The parameters a and b can be obtained by fitting PVT experimental data. The average oil compressibility over the pressure range from the initial formation pressure p_i to the current pressure p can be calculated with Equation (3):

$$C_{o,avg} = \frac{\int_{p_i}^{p} C_o dp}{p - p_i} = \frac{b}{p - p_i} \ln \frac{p}{p_i} \tag{7}$$

$C_{o,avg}$ represents the average oil compressibility when the average formation pressure decreases from p_i to p. This approach of utilizing an overall average is particularly effective when the pressure drop is modest, as it offers a satisfactory approximation.

Figure 1 shows a comparison between the oil compressibility (C_o) and its averaged counterpart ($C_{o,avg}$). Here, C_o represents the oil compressibility obtained from fitting PVT experimental data, while $C_{o,avg}$ represents the average oil compressibility of the same sample calculated using Equation (7). When the pressure drop is great, the disparity between $C_{o,avg}$ and C_o increases significantly. Persisting with this averaging approach under such conditions may lead to an underestimation of the elastic energy of crude oil, consequently resulting in incorrect evaluations of dynamic reserves.

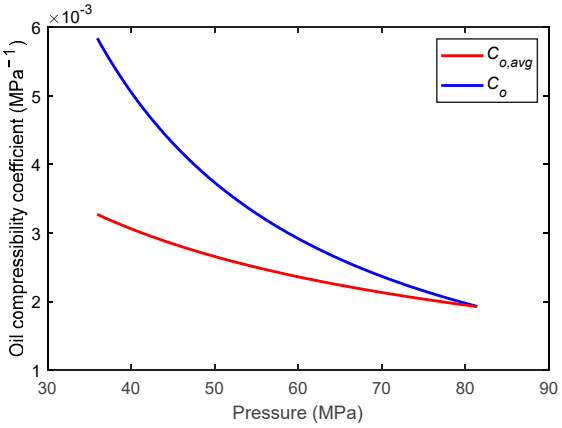


Figure 1. Comparison of C_o and $C_{o,avg}$.

To avoid the above-mentioned situation as much as possible, a segmented elastic-drive material balance equation is established. During the production cycle spanning from t_{n-1} to t_n, the average pressure decreases from p_{n-1} to p_n. The oil rate of $q_{o,n}$ and the water rate of $q_{w,n}$ during this interval depend on the elastic energy of the underground crude oil and rock at the initial moment t_{n-1}. Consequently, Equation (1) can be modified into

$$q_{o,n}B_{o,n} + q_{w,n}B_w = \left(N - N_{p,n-1}\right)B_{o,n-1}(p_{n-1} - p_n)\left(\overline{C}_{o,n} + \frac{C_f + C_w S_{wi}}{1 - S_{wi}}\right) \tag{8}$$

where $q_{o,n}$ is the oil rate from t_{n-1} to t_n, m^3; $q_{w,n}$ is the water rate from t_{n-1} to t_n, m^3; and $\overline{C}_{o,n}$ is the average oil compressibility under the average pressure from p_{n-1} to p_n, MPa^{-1}.

2.2. Water Invasion Stage

When water invasion occurs, oil and water production depends on water intrusion, underground crude oil expansion, pore shrinkage, and original formation-water expansion. Therefore, the material balance equation can be obtained:

$$N_p B_o + W_p B_w - W_e = N B_{oi}(p_i - p)\left(C_{o,avg} + \frac{C_f + C_w S_{wc}}{1 - S_{wc}}\right) \tag{9}$$

where W_e is the cumulative water influx, m^3.

The piecewise fitting method still modifies the material balance equation in terms of water invasion. During the production cycle spanning from t_{n-1} to t_n, the oil rate of $q_{o,n}$ and the water rate of $q_{w,n}$ depend on the elastic energy of the underground crude oil, rock, and water invasion at the initial moment t_{n-1}. So, Equation (9) can be expressed as

$$q_{o,n}B_{o,n} - (q_{we,n} - q_{w,n}) = (p_{n-1} - p_n)\left[\begin{array}{l} B_{o,n-1}(N - N_{p,n-1})\left(\frac{C_f + S_{wc}C_w}{1-S_{wc}} + \overline{C}_{o,n}\right) \\ +(W_e - W_p)_{n-1}C_w \end{array}\right] \quad (10)$$

where $q_{we,n}$ is the water influx from t_{n-1} to t_n, m^3.

3. Calculation of Rock Compressibility, Dynamic Reserves, and Aquifer Size

3.1. Identification of Water Invasion Stage

Water invasion can typically be identified by analyzing the alterations in the slope of the average pressure versus the cumulative oil production curve. According to Equation (1), the relationship between the cumulative oil production and pressure drop adheres to a linear pattern under conditions with no water invasion. When water invasion occurs, the equivalent cumulative oil production results in a reduced average formation-pressure drop, because water influx counteracts volumetric variations in both oil and pore spaces in the reservoir. Consequently, the absolute slope of the pressure drop versus cumulative production curve diminishes, with the degree of slope reduction directly reflecting the severity of water invasion.

The Pruned Exact Linear Time (PELT) algorithm represents a well-established method for change point detection, extensively validated through peer-reviewed studies in statistical time series analysis [29–31]. It has also been used in the field of petroleum engineering to prove its reliability [32–34].

The PELT algorithm facilitates the artificial specification of the number of change points, thereby allowing the stages delineated by these points to correspond with the actual water invasion characteristics of the reservoir. The fundamental principle underlying this approach is that when a change point is introduced into the observed sequence of the data vector, the value of the overall sequence's loss function will decrease. Specifically, there exists a constant K so that for all $i < s < j$,

$$C(y_{i+1:s}) + C(y_{s+1:j}) + K \leq C(y_{i:j}) \quad (11)$$

where C is the loss function, and $y_{i+1:s}$ is the items $i + 1$ to s in the data vector.

Let the observed time series data be denoted as $y = (y_1, y_2, \ldots, y_n)$, where potential change points occur at positions $\tau_1, \tau_2, \ldots, \tau_m$. The loss function, penalty term, and objective function can be defined as

$$C = \sum_{i=0}^{m} \sum_{s=\tau_i+1}^{\tau_{i+1}} [y_s - (\alpha_i + \beta_i s)]^2 + \theta \quad (12)$$

$$\theta = k \ln n \quad (13)$$

$$F(s) = \min_{\tau \leq s}[F(\tau) + C(y_{\tau+1:s}) + \theta] \quad (14)$$

where α_i and β_i represent the intercept and slope of the i-th segment estimated by the least squares method, respectively, and k is the number of additional parameters (two additional parameters per change point).

A candidate point s is excluded from subsequent calculations if it satisfies

$$F(s) + C\left(y_{s+1:j}\right) \geq F(j) \tag{15}$$

This pruning criterion ensures computational efficiency by eliminating non-optimal candidates early. The ruptures library in Python 3.9 or the ischange function in MATLAB R2019b can be used for the detection of change points based on the PELT algorithm [35]. In this paper, the results of identifying the change point in the pressure versus cumulative oil production curve for Well A utilizing this methodology are given.

Figure 2 illustrates that the variation curve of average formation pressure in relation to cumulative oil production is segmented into three distinct stages. The first stage denotes a period characterized by the absence of water invasion, with the slope exhibiting the largest absolute value. This observation indicates that the cumulative oil production per unit pressure drop is minimized during this stage. The second stage corresponds to the initial water invasion stage, wherein pressure may not have fully influenced the water body. Nonetheless, due to the onset of water invasion, there is a slight decrease in the absolute value of the slope. The third stage signifies full water invasion, during which the cumulative oil production per unit pressure drop attains its maximum. The aquifer size derived from this segment of the data can be seen as the maximum volume of the water body.

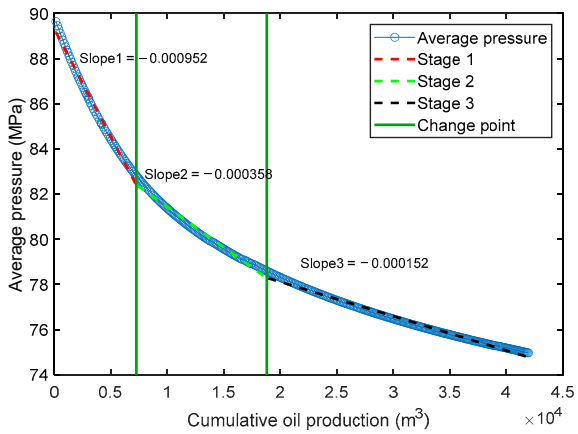


Figure 2. The results of dividing water invasion into stages for Well A.

3.2. Estimation of Rock Compressibility and Dynamic Reserves

Based on the results of dividing water invasion into stages, the rock compressibility and dynamic reserves can be obtained by using the data of the no water invasion stage. Equation (8) can be rewritten as follows:

$$Z = NX - \frac{1}{Y + \frac{C_f + C_w S_{wc}}{1 - S_{wc}}} \tag{16}$$

where

$$X = \frac{B_{o,n-1}(p_{n-1} - p_n)}{q_{o,n}B_{o,n} + q_{w,n}B_w} \tag{17}$$

$$Y = \frac{b}{p_n - p_{n-1}} \ln \frac{p_n}{p_{n-1}} \tag{18}$$

$$Z = N_{p,n-1} \frac{B_{o,n-1}(p_{n-1} - p_n)}{q_{o,n}B_{o,n} + q_{w,n}B_w} \tag{19}$$

X, Y, Z can be calculated according to the production data, and then the dynamic reserves and rock compressibility can be obtained by fitting. The calculation steps are as follows:

1. Set the value range of dynamic reserves and rock compressibility and give the corresponding initial value;
2. Calculate the right-hand side of Equation (16) according to the pressure and rate data to obtain Z';
3. Employ the Levenberg–Marquardt algorithm [36,37] to iteratively calculate the minimum residual sum between Z and Z' in a specified range of values.

3.3. Calculation of Aquifer Size

The reservoir's dynamic reserves and rock compressibility can be obtained by the calculations in Section 3.2. Rock compressibility can be used for both water and oil zones. Before the aquifer size is determined, the water influx is calculated according to the production data of the water invasion stage. It is assumed that water invasion in the oil region is driven by the elastic energy of formation water and pores in the water region.

$$W_e = \Delta V_w + \Delta V_{p,w} \tag{20}$$

where ΔV_w is the changing volume of the water body, m^3; and $\Delta V_{p,w}$ is the changing volume of pores in water region.

Water compressibility can be expressed as

$$C_w = \frac{1}{V_w}\frac{dV_w}{dp} \tag{21}$$

where C_w is the isothermal water compressibility, MPa^{-1}; and V_w is the water body's volume, m^3.

After the variables in Equation (21) are separated and integrated, assuming that the average formation pressure drops from the initial pressure p_i to p, the water volume in the water zone is as follows:

$$V_w = V_{wi}e^{C_w(p_i-p)} \tag{22}$$

where V_{wi} is the initial volume of the water body in the water zone, m^3.

Then, the changing volume of the water body can be expressed as

$$\Delta V_w = V_{wi} - V_w = V_{wi}\left[e^{C_w(p_i-p)} - 1\right] \tag{23}$$

The pore volume change in the water zone can be derived from the definition of rock compressibility:

$$C_f = -\frac{1}{V_p}\frac{dV_p}{dp} \tag{24}$$

where V_p is the pore volume in the water zone, m^3.

For Equation (24), variables are separated and integrated, and the change in rock pore volume can be expressed as

$$\Delta V_p = V_{pi} - V_p = V_{pi}\left[1 - e^{-C_f(p_i-p)}\right] \tag{25}$$

Substituting Equations (23) and (25) into Equation (20) gives the following relationship:

$$W_e = V_{wi}\left[e^{C_w(p_i-p)} - 1\right] + V_{pi}\left[1 - e^{-C_f(p_i-p)}\right] \tag{26}$$

The pore space in the water zone is filled with formation water, so the pore volume in the water zone is equal to the water body's volume. By defining the aquifer size as the ratio of the water zone volume to the oil zone volume, the relationship between the cumulative water influx and aquifer size can be obtained:

$$W_e = n\frac{NB_{oi}}{1-S_{wi}}\left[e^{C_w(p_i-p)} - e^{-C_f(p_i-p)}\right] = n \cdot f(p) \quad (27)$$

The water influx from t_{n-1} to t_n can be calculated using Equation (10). The cumulative water influx during the water invasion stage can be obtained after summing the computed results, and the aquifer size can be obtained with Equation (27).

4. Method Validation

A numerical model is developed to validate the proposed method by generating essential input data. The model configuration features a two-layer system, with the upper zone containing pure oil and the lower zone comprising pure water. A constant liquid production rate of 100 m^3/d is maintained while constraining the bottom-hole pressure to a minimum of 40 MPa. Key reservoir properties and operational parameters governing the simulation are summarized in Table 1.

Table 1. Basic parameters for the numerical model.

Parameter	Value	Parameter	Value
Grid number in x direction	50	Permeability in x direction (mD)	50
Grid number in y direction	50	Permeability in y direction (mD)	50
Grid number in z direction	40	Permeability in z direction (mD)	5
Grid size (m)	10	Porosity	0.05
Initial pressure (MPa)	80.4	Rock compressibility (MPa^{-1})	0.0003
Original oil in place (m^3)	621,078	Water volume (m^3)	309,845

Based the simulated production data, the proposed computational workflow is implemented to determine the rock compressibility, dynamic reserves, and aquifer size, respectively, and compare the differences between the calculated and output results of the model.

Figure 3 presents the results of the segmentation of water invasion stages as determined by the PELT algorithm. Similarly to Figure 2, three stages are established: the no water invasion stage, the initial water invasion stage, and the full water invasion stage. The figure indicates that the ratio of the pressure drop to cumulative oil production is subject to change following the beginning of water invasion. The slope observed in stage 2 is considerably larger than that in stage 1. However, this difference is not as noticeable when compared to stage 3. This suggests that the water volume in the model is relatively limited, and the pressure spreads quickly throughout the water body.

To calculate the oil volume factor and compressibility using Equation (6) and Equation (7), it is essential to fit the experimental data of the oil volume factor. Figure 4 presents the fitting results for the oil volume factor. The saturation pressure of the fluid utilized for fitting is 32.25 MPa. The figure demonstrates a power law relationship between the crude oil volume factor and pressure, with an R^2 value of 0.998. This indicates that the derivation of Equation (6) is valid, where the coefficient b is -0.1897.

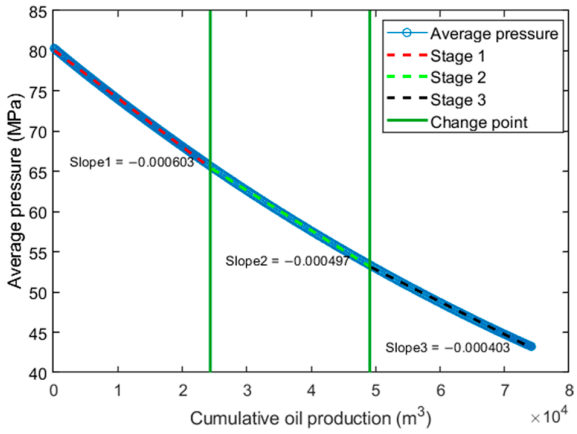


Figure 3. Average pressure versus cumulative oil production for the numerical model.

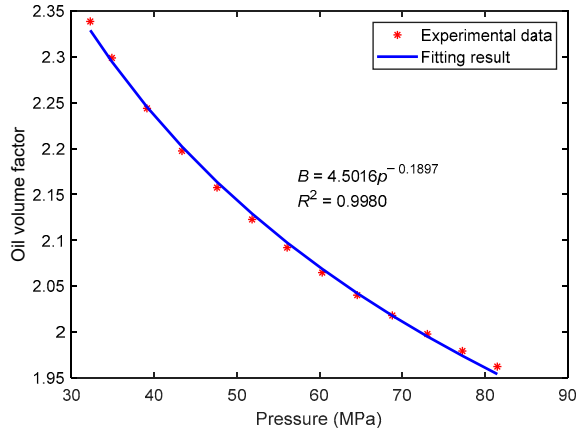


Figure 4. The fitting results for the oil volume factor.

The method proposed in this paper is applied to the data from the first stage to calculate dynamic reserves and rock compressibility, followed by a comparison with the input parameters of the numerical model. Equations (16)–(19) are employed to compute the values of X, Y, Z, and Z', with the results of the fitting and calculations presented in Figure 5 and Table 2, respectively. Figure 5 illustrates that the Levenberg–Marquardt algorithm has a good fitting effect. The difference at the front end of the curve may result from the transient flow in the reservoir in early-stage production, during which the material balance method is not applicable. Table 2 shows the calculation results for dynamic reserves and rock compressibility, indicating that the relative error between the calculated rock compressibility and the input value is 0.67%, while the relative error for dynamic reserves stands at 0.34%.

After dynamic reserves and rock compressibility are calculated, the cumulative water influx can be obtained using Equation (10). Subsequently, the function $f(p)$ on the right side of Equation (27) is computed. The values of W_e and $f(p)$ are then fitted, segregating the data according to the divided water invasion stages. The slope of the resulting linear relationship signifies the aquifer size.

As shown in Figure 6, the aquifer sizes corresponding to the second and third stages are 0.2512 and 0.2578, respectively. The minimal difference indicates that the reservoir's water volume is relatively limited. In the actual numerical model, the aquifer size is 0.2548, which results in a calculated relative error of only 1.19%.

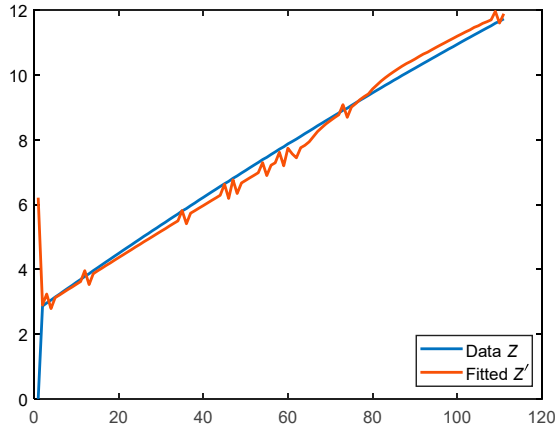


Figure 5. The fitting results of calculated parameter Z'.

Table 2. Calculation results and relative errors of dynamic reserves, rock compressibility, and aquifer size.

Parameter	Type	Value	Relative Error
Dynamic reserves (m^3)	Fitting Validation	618,964.17 621,078	0.34%
Rock compressibility (MPa^{-1})	Fitting Validation	0.000333 0.000302	0.67%
Aquifer size	Fitting Validation	0.2578 0.2548	1.19%

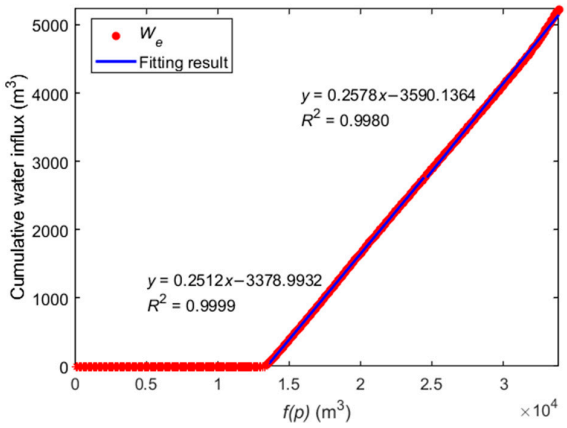


Figure 6. Cumulative water influx versus calculated parameter $f(p)$ for the numerical model.

5. Application to a Field Case

With Well A taken as the case, the dynamic reserves, rock compressibility, and aquifer size are calculated using the modified material balance method. The water invasion stage identification of Well A is shown in Figure 2. According to the PVT report of Well A, the relationship between the oil volume factor and pressure is fitted. The formation-water saturation (S_{wc}) for Well A is 0.2, while the formation-water compressibility (C_w) is 4.5×10^{-4}/MPa. The dynamic reserves and rock compressibility calculated for Well A are 74.41×10^4 m^3 and 2.8×10^{-4}/MPa, respectively (Table 3). The initial aquifer size is calculated to be 2.51, escalating to a final aquifer size of 8.22 (Figure 7).

Table 3. Calculation results of rock compressibility, dynamic reserves, and aquifer size of well A.

Fitting Parameter b of Oil Volume Factor	Rock Compressibility (10^{-4}/MPa)	Dynamic Reserves (10^4 m^3)	Aquifer Size
−0.075	0.00028	74.41	8.22

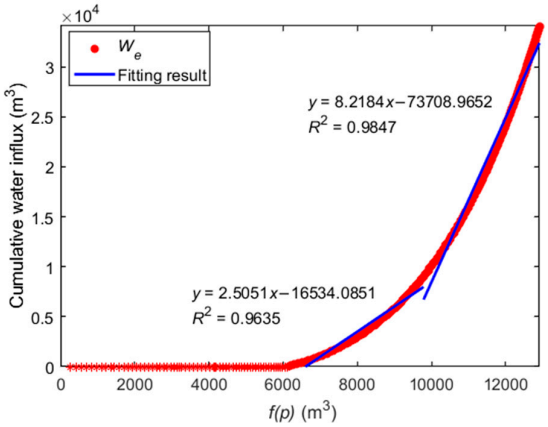


Figure 7. Cumulative water influx versus calculated parameter $f(p)$ for Well A.

6. Conclusions

An enhanced material balance equation is presented for fractured–vuggy reservoirs with a bottom aquifer, integrating the PELT algorithm and nonlinear least squares method. This equation facilitates the calculation of rock compressibility, dynamic reserves, and aquifer size. The validity of the model has been substantiated through the numerical model, yielding the following conclusions:

(1) The method replaces the traditional averaged oil compressibility with a pressure-dependent power law model for oil volume factors. The error caused by large pressure drops is eliminated by fitting a segmented elastic-drive material balance equation;

(2) Integrated parameter inversion simultaneously resolves rock compressibility, dynamic reserves, and aquifer size using only production data (oil/water rates, pressure), bypassing reliance on injection data or laboratory rock properties;

(3) The PELT algorithm is employed to automate water invasion stage segmentation, objectively identifying no water invasion, initial water invasion, and full water invasion stages by analyzing average pressure-cumulative production slopes, minimizing subjective bias. Rock compressibility and dynamic reserves can be calculated using data from the no water invasion stage, and the aquifer size can be determined from the water invasion stage data;

(4) Rock compressibility and dynamic reserves can be ascertained via the nonlinear least squares method with relative errors below 1%. The aquifer size obtained for the linear regression of the cumulative water influx against the pressure-dependent function yields an error of 1.19%;

(5) Due to its connectivity and production regulation, the reservoir's water body may not be entirely impacted by pressure, resulting in a gradual increase in the aquifer size until stabilization.

Author Contributions: Methodology, B.F.; Validation, Y.J. and B.L.; Investigation, W.Y.; Writing—original draft preparation, B.F.; Writing—review and editing, Y.T.; Funding acquisition, Y.J. and Q.Z. All authors have read and agreed to the published version of the manuscript.

Funding: This research was funded by Research on New Mechanisms and Methods for Enhancing Recovery in Condensate Gas Reservoirs (2023ZZ0406) and Research on New Methods for Dynamic Evaluation of Ultra-Deep Fractured-vuggy Carbonate Reservoirs (2024DJ1003).

Data Availability Statement: The raw data supporting the conclusions of this article will be made available by the authors on request.

Conflicts of Interest: Author Wei Yu was employed by SimTech LLC. The remaining authors declare that the research was conducted in the absence of any commercial or financial relationships that could be construed as a potential conflict of interest.

References

1. Wang, X.; Wang, J.; Cao, Y.; Han, J.; Wu, K.; Liu, Y.; Liu, K.; Xie, M. Characteristics, formation mechanism and evolution model of Ordovician carbonate fault-controlled reservoirs in the Shunnan area of the Shuntuogole lower uplift, Tarim Basin, China. *Mar. Petrol. Geol.* **2022**, *145*, 105878. [CrossRef]
2. Ostad, H.; Mohammadi, Z.; Raeisi, E.; Azimi, M.H.; Liso, I.S.; Parise, M. An integrated approach for characterization of a fractured-rock carbonate aquifer in the Zagros Region of Iran. *J. Hydrol.* **2024**, *640*, 131681. [CrossRef]
3. Wu, W.P.; Yang, M.; Ma, D.C.; Hou, J.R.; Liang, T.; Qu, M.; Tan, T.; Yang, B.; Ma, G.R. Towards in-depth profile control using s-MPG synergy with MSRG in fractured-vuggy carbonate reservoirs. *Petrol. Sci.* **2024**, *22*, 324–337. [CrossRef]
4. Islamov, S.; Bondarenko, A.V.; Gabibov, A.F.; Mardashov, D. Polymer compositions for well killing operation in fractured reservoirs. In *Advances in Raw Material Industries for Sustainable Development Goals*; Taylor & Francis: London, UK, 2020. [CrossRef]
5. Wu, Y.S.; Liu, H.H.; Bodvarsson, G.S. A triple-continuum approach for modeling flow and transport processes in fractured rock. *J. Contam. Hydrol.* **2004**, *73*, 145–179. [CrossRef]
6. Arbogast, T.; Gomez, M.S.M. A discretization and multigrid solver for a Darcy-Stokes system of three dimensional vuggy porous media. *Computat. Geosci.* **2009**, *13*, 331–348. [CrossRef]
7. Wu, Y.S.; Di, Y.; Kang, Z.; Fakcharoenphol, P. A multiple-continuum model for simulating single-phase and multiphase flow in naturally fractured vuggy reservoirs. *J. Pet. Sci. Eng.* **2011**, *78*, 13–22. [CrossRef]
8. Zhang, N.; Yao, J.; Xue, S.; Huang, Z. Multiscale mixed finite element, discrete fracture-vug model for fluid flow in fractured vuggy porous media. *Int. J. Heat Mass Tran.* **2016**, *96*, 396–405. [CrossRef]
9. Wang, Y.; Hou, J.R.; Tang, Y.; Song, Z.J.; You, Z.J. Application of modified Dykstra-Parsons method to natural bottom-water drive in non-communicating fractured-vuggy reservoir. *J. Pet. Sci. Eng.* **2018**, *167*, 682–691. [CrossRef]
10. Yan, X.; Huang, Z.; Yao, J.; Zhang, Z.; Liu, P.; Li, Y.; Fan, D. Numerical simulation of hydro-mechanical coupling in fractured vuggy porous media using the equivalent continuum model and embedded discrete fracture model. *Adv. Water Resour.* **2019**, *126*, 137–154. [CrossRef]
11. Shao, R.; Di, Y.; Wu, D.; Wu, Y.-S. An Integrally Embedded Discrete Fracture Model for Flow Simulation in Anisotropic Formations. *Energies* **2020**, *13*, 3070. [CrossRef]
12. Idogun, I.; Jeboda, O.; Charles, D.; Ufomadu, H. Material Balance Modeling and Performance Prediction of a Multi-Tank Reservoir. In Proceedings of the SPE Nigeria Annual International Conference and Exhibition, Lagos, Nigeria, 4–6 August 2015. [CrossRef]
13. Alcantara, R.; Ham, J.M.; Paredes, J.E. Applications of Material Balance for Determining the Dynamic Performance of Fractures in a Dual-Porosity System in HP-HT Reservoirs. In Proceedings of the SPE Russian Petroleum Technology Conference, Moscow, Russia, 16–18 October 2017. [CrossRef]
14. Molokwu, V.C.; Onyekonwu, M.O. Multi-Tank Material Balance Analysis in Heterogeneous Oil Reservoirs. In Proceedings of the SPE Nigeria Annual International Conference and Exhibition, Lagos, Nigeria, 31 July–2 August 2017. [CrossRef]
15. Wang, Z.H.; Wang, Z.D.; Zeng, F.H.; Guo, P.; Xu, X.Y.; Deng, D. The material balance equation for fractured vuggy gas reservoirs with bottom water-drive combining stress and gravity effects. *J. Nat. Gas Sci. Eng.* **2017**, *44*, 96–108. [CrossRef]
16. Fuentes-Cruz, G.; Vásquez-Cruz, M.A. Reservoir performance analysis through the material balance equation: An integrated review based on field examples. *J. Pet. Sci. Eng.* **2022**, *208*, 109377. [CrossRef]
17. Istayeva, U.; King, G. Application of the Extended Dynamic Material Balance Method to a Super Giant Carbonate Oilfield. In Proceedings of the SPE Annual Caspian Technical Conference and Exhibition, Astana, Kazakhstan, 12–14 November 2014. [CrossRef]
18. Han, G.F.; Liu, Y.W.; Sun, L.; Liu, M.; Gao, D.P.; Li, Q. Determination of pore compressibility and geological reserves using a new form of the flowing material balance method. *J. Pet. Sci. Eng.* **2019**, *172*, 1025–1033. [CrossRef]
19. Yao, C.; Yan, R.; Zhou, F.; Zhang, Q.; Niu, G.; Chen, F.; Cao, W.; Wang, J. A Novel Method to Calculate Water Influx Parameters and Geologic Reserves for Fractured-Vuggy Reservoirs with Bottom/Edge Water. *Energies* **2024**, *17*, 2822. [CrossRef]

20. Obot, N.; Eme, V. Application of Fluid Contact Match in Material Balance Study in a Water Injection Reservoir to Estimate STOOIP and Initial Reservoir Contacts. In Proceedings of the SPE Nigeria Annual International Conference and Exhibition, Lagos, Nigeria, 6–8 August 2018. [CrossRef]
21. Chen, L.; Jia, C.; Zhang, R.; Yue, P.; Jiang, X.; Wang, J.; Su, Z.; Xiao, Y.; Lv, Y. High-pressure capacity expansion and water injection mechanism and indicator curve model for fractured-vuggy carbonate reservoirs. *Petroleum* **2024**, *10*, 511–519. [CrossRef]
22. Yue, P.; Xie, Z.W.; Liu, H.H.; Chen, X.F.; Guo, Z.L. Application of water injection curves for the dynamic analysis of fractured-vuggy carbonate reservoirs. *J. Pet. Sci. Eng.* **2018**, *169*, 220–229. [CrossRef]
23. Wang, Y.; Jiang, H.Q.; Li, J.J. Study on Water Injection Indicator Curve Model in Fractured Vuggy Carbonate Reservoir. *Geofluids* **2021**, *2021*, 5624642. [CrossRef]
24. Zhang, Q.; Li, Y.; Wang, D.G.; Zhang, J.; Wang, Q.; Bao, R.F. A novel dynamic reserve evaluation method by division between oil and water in isolated fractured-caved carbonate reservoirs. *J. Pet. Sci. Eng.* **2022**, *214*, 110440. [CrossRef]
25. Yildiz, T. Prediction of In-Situ Formation Compressibility from Production Data. In Proceedings of the SPE/ISRM Rock Mechanics in Petroleum Engineering, Trondheim, Norway, 8–10 July 1998. [CrossRef]
26. Kegang, L.; Jun, H.; Peng, P.; Xiao, N. A New Method to Determine Pore Compressibility. In Proceedings of the 48th U.S. Rock Mechanics/Geomechanics Symposium, Minneapolis, Minnesota, 1–4 June 2014.
27. Zhu, S.Y.; Du, Z.M.; Li, C.L.; You, Z.J.; Peng, X.L.; Deng, P. An analytical model for pore volume compressibility of reservoir rock. *Fuel* **2018**, *232*, 543–549. [CrossRef]
28. Vazquez, M.; Beggs, H.D. Correlations for Fluid Physical Property Prediction. *J. Pet. Technol.* **1980**, *32*, 968–970. [CrossRef]
29. Killick, R.; Fearnhead, P.; Eckley, I.A. Optimal Detection of Changepoints with a Linear Computational Cost. *J. Am. Stat. Assoc.* **2012**, *107*, 1590–1598. [CrossRef]
30. Truong, C.; Oudre, L.; Vayatis, N. Selective Review of Offline Change Point Detection Methods. *Signal Process.* **2020**, *167*, 107299. [CrossRef]
31. Yan, Q.; Sun, Z.; Gan, Q.; Jin, W.-L. Automatic identification of near-stationary traffic states based on the PELT changepoint detection. *Transport. Res. B-Meth.* **2018**, *108*, 39–54. [CrossRef]
32. Ruzhnikov, A.; Guillot, V.; Corona, M. Real-Time Evaluation of the Lost Circulation Zone Based on a Changepoint Analysis of the Mechanical Specific Energy and Standpipe Pressure. In Proceedings of the International Petroleum Technology Conference, Dhahran, Saudi Arabia, 12 February 2024. [CrossRef]
33. Shakirov, A.B.; Lipko, A.; Mezghani, M. Automated Well Log-Based Prediction of Formation Tops: Case Study of Norway Offshore Data. In Proceedings of the ADIPEC, Abu Dhabi, United Arab Emirates, 2–5 October 2023. [CrossRef]
34. Sinha, S.; Kiran, R.; Tellez, J.; Marfurt, K. Identification and Quantification of Parasequences Using Expectation Maximization Filter: Defining Well Log Attributes for Reservoir Characterization. In Proceedings of the SPE/AAPG/SEG Unconventional Resources Technology Conference, Denver, CO, USA, 22 July 2019. [CrossRef]
35. Hwang, Y.; Kwak, S.; Jyoti; Kim, J. Optimal time-dependent SUC model for COVID-19 pandemic in India. *BMC Infect. Dis.* **2024**, *24*, 1031. [CrossRef]
36. Levenberg, K.Q. A Method for The Solution of Certain Non-Linear Problem in Least Squares. *Quart. Appl. Math.* **1944**, *11*, 93–101. [CrossRef]
37. Marquardt, D.W. An Algorithm for Least-Squares Estimation of Nonlinear Parameters. *J. Soc. Ind. Appl. Math.* **1963**, *11*, 431–441. [CrossRef]

Disclaimer/Publisher's Note: The statements, opinions and data contained in all publications are solely those of the individual author(s) and contributor(s) and not of MDPI and/or the editor(s). MDPI and/or the editor(s) disclaim responsibility for any injury to people or property resulting from any ideas, methods, instructions or products referred to in the content.